UNIVERSITY OF CALIFORNIA,

IRVINE

Characterization of Bifunctional ORR/OER Catalysts in Alkaline Media for Metal Air Batteries (MAB)

MASTER'S THESIS

Master's Degree in

Chemical and Biomolecular Engineering

By

John Lee

Thesis Committee:

Professor Plamen Atanassov, Chair

Associate Professor Iryna Zenyuk

Associate Professor Shane Ardo

2022

DEDICATION

To

My loving parents, grandmother, and my caring sisters and brother

In recognition of your endless love, encouragement, and extreme support during

Happy and tough times

TABLE OF CONTENTS

Acknowledgements

First and foremost, I would like to give my most sincere and deepest appreciation to my committee chair, Professor Plamen Atanassov, for his guidance in research and life. Without his guidance and persistent help, this thesis would not have been possible. I am very grateful to him for providing me this opportunity to work with him on research projects.

I would like to thank our postdoctoral fellow Dr. Pongsarun Satjaritanun for his expertise in preparation and testing our catalysts in his developed Zn-air battery. I would also like to thank my fellow graduate students in the Atanassov Lab group for their immense help and support. This thesis would not have been complete without their guidance.

In addition, I would like to thank our collaborator of this project, CDTi Advanced Materials, Inc, for providing us the bifunctional catalysts. I thank University of California, Irvine for providing this opportunity to achieve a master's degree.

This work has been funded by CDTi Advanced Materials, Inc. and the National Fuel Cell Research Center (NFCRC)

Characterization of Bifunctional ORR/OER Catalysts

in Alkaline Media for Metal Air Batteries (MAB)

by

John Franklin Lee

B.S., Chemical Engineering, New Mexico Institute of Mining and Technology, Socorro, 2018

M.S., Chemical and Biomolecular Engineering, University of California, Irvine, 2022

Abstract

Metal-air batteries (MAB) are becoming a revived interest because of their high theoretical energy density, low-cost, and environmentally friendly nature. They have wide range of applications from portable transportation to stationary applications. However, commercialization of this technology is hindered by the limitations associated with design: the metal anode, air cathode, and electrolyte.

Commercial benchmark catalysts at the cathode and anode are platinum nanoparticles over carbon-based supports and iridium oxide particles, respectively. However, carbon supports are highly susceptible to corrosion resulting in major performance losses. These metals are also expensive, limited, and difficult to obtain. Hence, corrosion-resistant support materials or an alternative metal are needed. In this study, catalytic activity of a library of transition metal oxides with various supports is explored.

All the catalysts were characterized physically and electrochemically to understand their morphological and electrocatalytic properties towards oxygen reduction reaction and oxygen evolution reaction.

The oxygen reduction reaction activity, investigated in aqueous 1 M KOH electrolyte, using rotating disk electrode showed worse performance than benchmark Pt/C. However, the oxygen evolution reaction activity surpassed performance of industrial catalyst IrO_x. The best performing catalyst in nickel iron oxides and nickel cobalt oxides, neglecting carbon supports, are also investigated in MABs.

This thesis provides an exploration of novel bifunctional catalysts tested electrochemically in aqueous 1 M KOH and aqueous 2 M NaCl. The best performing catalysts are then tested in a Zinc-Air battery in aqueous 1 M KOH.

Chapter 1. General Introduction

1.1 Current Challenges in Energy

In 2021, the US Environmental Information Administration (EIA) reported about 4,103 billion kilowatt-hours (kWh) of electricity were generated at electricity generation facilities. About 61% of this electricity generation was from fossil fuels. About 19% was from nuclear energy, and about 20% was from renewable energy sources.[1]

While there is still ample supply of natural resources, data over the past century shows there is a steady decline.[2] As the world continues to be depleted of its resources, it becomes necessary to find more reliable and abundant energy sources to satisfy the people's needs. Renewable energy sources such as solar energy, wind energy, geothermal, and hydroelectric energy could fulfill the requirements and reach the energy demands without causing any detrimental damages to the environment. However, the primary concern for renewable energy sources is their lack of stability. Most renewable sources rely on climate conditions such as the wind and the sun which are not available throughout the entire day. Thus, energy storage systems must be implemented to assist this issue.

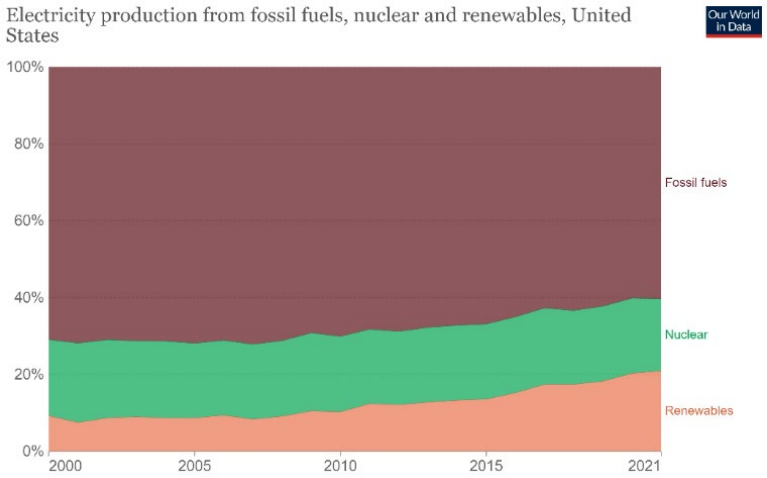

Figure 1: United States electricity production from energy sources from 2000 to 2021 based on Our World in Data (2022)

Of the many energy storage devices, lithium-ion batteries have made a large impact. They have high efficiency and are available in different sizes. However, they still have limitations in transportation. With the demand to promote electrical transportation and grid-scale stationary energy storage increasing, new chemistry and systems are being actively sought. With conventional lithium-ion technology, it is difficult to achieve long driving ranges in electrical vehicles because of its low energy density.

Metal-air batteries (MABs) are a worthy candidate as an energy storage device. In comparison to lithium-ion batteries, they have a larger theoretical energy density.[5-7] Research on MABs have been around even before lithium-ion batteries. [3] The first zinc-air battery was invented in 1878 and it was even commercialized in 1932.[4] Following that, different metal-air batteries with nonaqueous electrolytes were made. The development of MABs were greatly hindered by problems associated with the components because none of them were at a stage for large-scale industrial development.

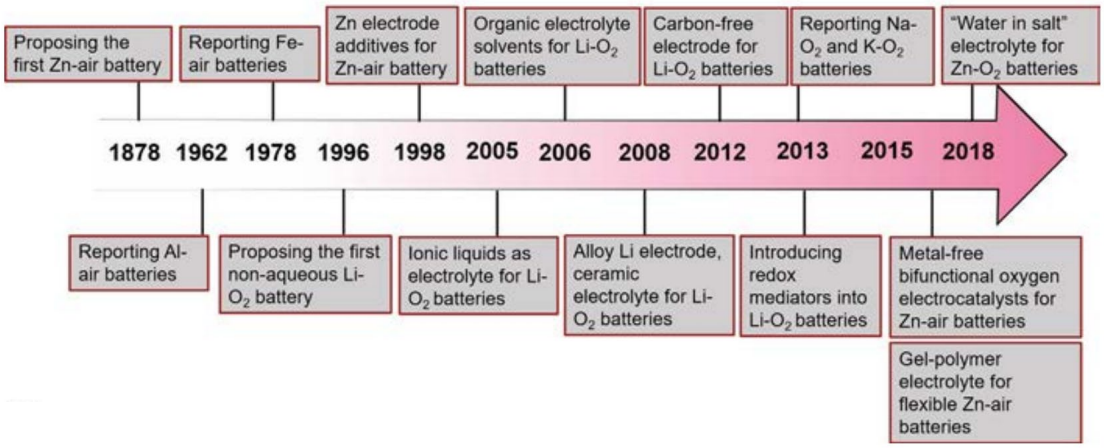

Figure 2: Timeline of research progress in metal-air batteries.

1.2 Metal-air Batteries

Metal-air batteries can be subdivided into primary and secondary batteries. Primary batteries are non-rechargeable batteries, designed to be a one-time usage once they discharge energy. As the primary cell is used, chemical reactions in the battery use up the chemicals that generate power. Once there are no more chemicals, the battery stops producing electricity. The benefits of primary batteries are they are compact, cheap, and applicable to a wide range of portable equipment. A secondary battery is rechargeable, where it may be electrically recharged after its discharge phase. This can happen with reversible redox reactions, and the reversible reactions complement the charge-discharge functions.

Metal-air batteries combine the structure features of conventional batteries and the concept of fuel cells. A typical metal-air battery system consists of a pure metal or metal alloy electrode as the anode, and an air electrode for oxygen involved reactions as the cathode. Electrolyte runs between these anodes serving as ion conductors allowing efficient ion transportation. The metal anode is made of either an alkali metal, alkaline earth metal, or first-row transition metal such as lithium, magnesium, or zinc. The electrolyte can be aqueous or non-aqueous depending on the anode metal. The air-breathing cathode has a porous architecture with a carbon-based covering that permits continuous oxygen supply from surrounding air.

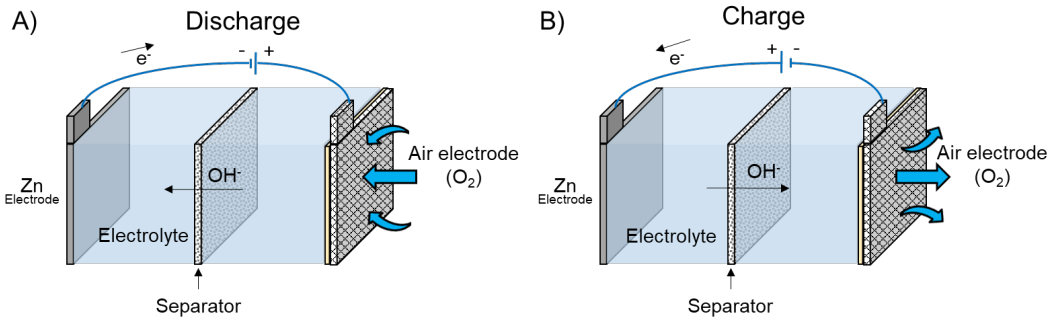

Figure 3: Schematic of a metal-air battery, specifically for zinc during charge and discharge phases.

1.3 Oxygen Electrodes

The development of efficient bifunctional catalysts has attracted significant interest for rechargeable metal-air batteries of further improved performance. Metal-air batteries should effectively reduce oxygen during the discharge cycle and evolve oxygen during the charge cycle.[8] During discharge and charge processes, oxygen reduction reactions (ORR) and oxygen evolution reactions (OER) occur on the surface of the air electrode. The working principle for metal-air batteries is the electrochemical reaction that occur between oxygen and metals:

Anode: $M \leftrightarrow M^{n^+} + ne^-$

Cathode: $O_2 + 2H_2O + 4e^- \leftrightarrow 4OH^-$

To date, the commercial noble metals catalysts, such as platinum or iridium/ruthenium-based materials exhibit the best activities on ORR or OER. Much research has gone into the design and utilization of these materials, with variations on multiple parameters to increase their efficiency. The drawbacks are these materials are scarce, expensive, and the mining resources are located in politically unstable countries. Accordingly, it is desired to create economical and functional substitutes derived from inexpensive materials such as transition metal oxides.

1.4 Carbon Supports and their Downsides

Transition metals have low conductivities, which will result in a drop of activity in the electrocatalytic reactions. In electrocatalysis, carbon is commonly used as support for dispersion of catalysts to boost charge transfer. Carbon has good electrical conductivity, relatively high surface area, and is affordable. Carbon can be used as a support to increase the conductivities for transition metal oxides. A major issue to deal with carbon are the mass transport limitations with carbon and catalyst. Mass transport losses are induced by the dense structure of carbon which

affects the interaction between Nafion polymer and catalyst particles. Carbon is also susceptible to severe electrochemical oxidation which will lower OER performance. Carbon corrosion can also cause dendrites and agglomerations of metals to form in metal-air batteries. For alkaline media, carbon reacts to form carbon dioxide. The carbon dioxide then reacts with hydroxide ions in the aqueous electrolyte to form carbonates. Carbonates precipitate into the gas diffusion electrode and block oxygen transport. This chemical reaction imposes a high potential on the electrodes using more of the active materials thus lowering the cell durability and overall performance.

1.5 Mixed Metal Oxide Supports, their Advantages and Implications

It is found that pure metal oxides or compounds such as spinels and perovskites possess high electrical conductivity and can be used without the addition of carbon because of their high intrinsic activity and compositional flexibility.[10-20]

1.6 Objectives of this Research

The main objective of this research is to discover and characterize bifunctional catalysts at the laboratory scale and observe their performance in metal-air batteries, specifically in zinc-air battery. The term, "bifunctional" means these catalysts must perform electrochemically in ORR and OER well, increasing the flexibility of their application. The objectives are:

- Novel bifunctional catalysts provided by CDTi Advanced Materials, Inc. will be investigated in physical and electrochemical characteristics.
- Ni-CoO_x electrocatalyst will be synthesized using NaOH method

- Investigation of the physico-chemical properties of these catalysts will be conducted using several characterization techniques
- Catalysts will be tested for their ORR and OER performance in aqueous basic electrolyte 1.0 M KOH
- ORR and OER results of catalysts will be summarized and compared against industrial Pt/C and Iridium Oxide catalysts
- Catalysts will be tested in Zinc-air battery for charge/discharge profiles
- Charge and discharge profiles of catalysts will be summarized and compared with Pt/C

Chapter 2. Motivation and Hypothesis

The research followed the path of: (i) design, (ii) synthesis and (iii) characterization. Design includes selecting promising candidates based on literature review. Synthesis methods are selected as a function of the precursors chosen and standard chemical laboratory practices, with modifications to achieve the highest performance in both ORR and OER. Characterization is achieved through standard laboratory techniques and has two parts: physical and electrochemical.

2.4 Catalyst Design

Many transitional metal oxides, such as perovskite, pyrochlore, and spinel oxides and their mixtures, have been studied thanks to their low cost and high catalytic activity.

2.4.1 Perovskites

Perovskite oxides have a general formula of ABO_3, where the A-site is a rare alkaline earth metal cation, and the B-site is a 3d transition metal cation. Substitution of the A-site and/or B-site metal cations could generate enriched oxygen deficiency/vacancy in the structure, which may significantly impact on their electronic structure and coordination chemistry, leading to enhanced ORR and OER activities. [21] Many perovskite oxides such as $CaMnO_3$[22], and $LaFeO_3$[23] have been investigated as air cathode catalysts for metal-air batteries. Perovskites benefit greatly with their high oxygen kinetics, electrical conductivity, and structural stability, but they are difficult to synthesize into nanoparticles, limiting their full potential and hindering large-scale application.

2.4.2 Spinels

Spinel oxides have the general formula of $A_xB_{3-x}O_4$, where B is a 3d transition metal cation. Spinel oxides are designed by a packed array of O^{2-} anions, with A^{2+} and B^{3+} cations

locating at the tetrahedral and octahedral sites, respectively. The cationic holes improve electric conductivity and increases the number of active sites for oxygen reactions. The best part about spinels are the redox reactions occurring in the alkaline metals and transition metal oxides. The reactions enable the spinel oxides to have incredible catalytic activities toward both ORR and OER. Previous research reported a methodology for nanocrystalline $M_xMn_{3-x}O_4$ spinel oxides with controlled formation of tetragonal or cubic structure.[24] The cubic structure outperforms tetragonal phase in ORR activity, but the tetragonal phase surpasses cubic phase in OER. DFT results show cubic phase have a stronger metal oxide bond in comparison with the tetragonal phase.

Between the two candidates for metal-air batteries, spinel oxides are the best choice due to their ability to adjust its structure formation to significantly increase catalytic activity. Spinel oxides can also become a hybrid catalyst adding conductive carbon materials with spinel oxide particles to enhance reaction kinetics and catalytic efficiency. By including oxide particles into the carbon fiber matrix, the formation of discharged products can be suppressed, increasing operation time for Zn-air batteries.

2.4.3 Catalyst Selection

For selection of spinel oxides, Ni is selected for the A-site metal and Co and Fe are selected for the B-site. Carbon support is also incorporated with the aim to further increase performance of oxides as bifunctional catalysts. Antimony doped with tin oxide supports will also be investigated as an alternative to carbon for OER reactions.

2.5 Catalyst Synthesis

Some of the challenges in synthesis are morphological control and catalyst durability. Morphological control includes consistent porosity, surface area, and overall physical characteristics. A catalyst's durability determines its reliability in a commercial device under operating conditions. In a metal-air battery, the catalyst is cycled numerous times, lowering its activity by each cycle.

2.6 Characterization

Physical and electrochemical characteristics of the catalysts were observed using scanning electron microscopy (SEM), transmission electron microscopy (TEM), x-ray diffraction (XRD), rotating disk electrode (RDE) and a multimeter.

Research was conducted in the following order of tasks:

- Synthesize a library of catalysts with differing ratios, supports, and metals
- Measure the resistance of catalysts using a current-voltage multimeter and calculate the conductance
- Measure the ORR/OER activities of catalysts
- Integrate catalysts into Zn-Air cells

Chapter 3. Metals

3.1 Library of Metal Oxide Supports

Metal Oxide electrocatalysts (#1 - #12) were supplied by CDTi Advanced Materials, Inc. The last catalyst (#14) was synthesized in lab for comparison with CDTi's catalyst #1 $NiCo_5O_x$ – unsupported.

Table 1. Library of Catalysts, ATO: antimony tin oxide

Sample number	Catalysts	Description
#1	$NiCo_5O_x$ - unsupported	Ratio: 1:5, Oxide only
#2	$NiCo_5O_x$/VulcanXC72R	Ratio: 1:5, On VC72 standard process
#3	$NiCo_5O_x$/VulcanXC72R*	Ratio: 1:5, On VC72 modification process
#4	$NiCo_2O_x$ - unsupported	Ratio: 1:2, Oxide only
#5	$NiFe_2O_x$/VulcanXC72R	Ratio: 1:2, On VC72 standard process
#6	$NiFe_2O_x$ - unsupported	Ratio: 1:2, Oxide only
#7	$NiFe_2O_x$/VulcanXC72R*	Ratio: 1:2, On VC72 modification process
#8	$NiFeO_x$ with ATO	Ratio 1:2
#9	Trimetal (Ni, Fe, Co) Oxide with ATO	250CA
#10	Trimetal (Ni, Fe, Co) Oxide with ATO	251CB
#11	Trimetal (Ni, Fe, Co) Oxide with ATO	2521A
#12	Trimetal (Ni, Fe, Co) Oxide with ATO	2531B
#13	NiOH and FeO_x with ATO	
#14	$NiCo_5O_x$ - unsupported	Coprecipitation method by NaOH

3.2 Synthesis of Ni-Co5 Oxide Support

A stoichiometric 5:1 amount of $Co(NO_3)_2 \cdot 6H_2O$ (Sigma-Aldrich, 98%, 3.64 g) and $Ni(NO_3)_2 \cdot 6H_2O$ (Sigma-Aldrich, 99%, 0.73 g) was dissolved in 150 mL of deionized water and stirred for 15 min with a magnetic stirrer. Aqueous 2 M NaOH (Sigma-Aldrich, 99%) solution was added under continuous stirring until the pH of the reaction medium reached a value higher than 12. A black precipitate formed immediately. The solution was stirred for an additional 1 hour, then left to stand for 12 hours. To remove any remaining nitrates, the solution was cleaned five times with deionized water using a centrifuge spun at 3000 RPM. The mixed precipitate was filtered, washed thoroughly and then dried at 80 ºC overnight. Finally, it was calcinated at a temperature of 325 ºC for 4 hours using a temperature increase rate of 4ºC/min.[27]

3.3 Transmission Electron Microscopy (TEM)

For Transmission Electron Microscopy (TEM) investigations, the catalyst was dispersed in isopropyl alcohol and deposited on top of a copper grid. After the isopropyl alcohol evaporated, the sample grid was mounted on a double tilt holder of the microscope. Any impurities were removed on the holder using Gatan Solarus Advanced Plasma Cleaning. The micrographs were obtained using field emission transmission electron microscopies JEOL JEM-2800 TEM and JEOL JEM-2100F.

3.4 Scanning Electron Microscopy (SEM)

Scanning electron microscopy (SEM) was performed on a FEI Magellan 400 XHR scanning electron microscope with a voltage of 20.0 kV and 0.40 nA. Catalyst powder was dispersed on carbon tape attached onto a stub holder of the microscope.

3.5 X-ray Diffraction (XRD)

X-ray diffraction (XRD) patterns for the precious metal free catalysts were measured on a Rigaku SmartLab X-ray Diffractometer (Cu Kα, $\lambda = 1.54$ Å) with Cu Kα radiation and a beta filter in the range of 10 – 90^{o} (2θ) with 40 kV voltage and 30 mA current.

3.6 Electrochemical Methods

3.6.1 Preparation of the electrochemical cell and the electrodes

On day of testing, the Teflon cell was cleaned vigorously with MilliQ water. For all tests for ZAB, the electrolyte solution was prepared by adding 200 mL of 1.0 M KOH into the cell. For all tests for Aluminum-air Battery, trials were repeated with 2.0 M NaCl and 0.5 M NaCl.

All the electrochemical measurements were carried out with the help of VSP-300 Biologic potentiostat in a three-electrode electrochemical cell set-up. The three electrodes used were a commercial reversible hydrogen electrode as the reference electrode (RE), a carbon/graphite rod with a gold wire connection as the counter electrode (CE), and a rotating ring disk electrode with glassy carbon disk (0.247 cm^2) and Pt ring with drop casted electrocatalyst suspension as the working electrode (WE).

Prior to testing, the working electrode was prepared by cleaning the electrode using alumina slurries followed by multi-step sonication of acetone, ethanol, isopropyl alcohol, then DI water. After cleaning the WE, it was stored in DI water prior to utilization. The reference electrode and counter electrode were stored in MilliQ water until day of testing and soaked in electrolyte on the day of testing.

3.6.2 Preparation of the electrocatalyst suspensions

The electrocatalyst ink suspensions were made to get a catalyst loading of 800 μg/cm^2. The ratio of iso-propyl alcohol (IPA) to MilliQ water is maintained as 1:1. The Nafion Ionomer (Ion Power, Inc.) to IPA volumetric ratio was kept as 1:12.

The electrochemical inks were sonicated for 1 to 2 hours until a homogeneous slurry was observed. The ink was then drop casted onto the glassy carbon electrode. 10 μL was deposited onto the electrode rotating at 250 rpm. Once fully deposited, the rotation rate was increased to 400 rpm and was dried using horizontal hot air flow. This process was repeated 1 more time, so that 20 μL of ink was deposited. Once the ink was fully dried, the electrode was submerged into N_2 saturated electrolyte and subjected to various electrochemical tests.

3.6.3 Electrochemical Impedance Spectroscopy (EIS)

EIS was measured at 0.40 V vs RHE in the frequency range of 1 MHz to 10 Hz with 7 points per decade. EIS tests were carried out for all electrocatalysts in order to understand the electrolyte resistance.

3.6.4 Cyclic Voltammetry (CV) in N_2- saturated Electrolyte

CVs were carried out under N_2 environment in the 3-electrode RDE setup. 50 sweeps of activation CVs were performed between 0.05 and 1.23 V vs RHE at a scan rate of 500 mV/s. When the surface is fully activated, 3 CVs were performed at a scan rate of 20 mV/s. The results were plotted using potential E vs RHE and current density (mA/cm^2).

3.6.5 Linear Sweep Voltammetry (LSV) in N_2-saturated Electrolyte and O_2- saturated Electrolyte

A baseline LSV from 0.1 to 1.05 V vs RHE in N_2 saturated electrolyte was performed at a scan rate of 5 mV/s at a rotation rate of 1600 RPM. After scan completion, the cell was saturated with O_2 for 10 minutes, then LSVs were performed with the same conditions at various rotation rates. The obtained results were plotted using E vs RHE and current density (mA/cm^2) after addressing the ohmic and activation overpotential losses.

To observe OER activity, an LSV was performed from 1 to 1.7 V vs RHE in O_2 saturated electrolyte at a scan rate of 5 mV/s at a rotation rate of 1600 RPM. The obtained results were plotted using E vs RHE and current density (mA/cm^2).

3.7 Zinc-air Battery Testing

3.7.1 Zinc-electrode Preparation

Zn foil with a thickness of 0.25 mm has been used as a reference zinc electrode and benchmark the test. In this work, the advanced hybrid zinc electrode has been synthesis by using the Zn-coated on the Zn-Cu mesh. The simple Zn-coated method was used to coat the metallic zinc powder to the current collector. The zinc ink was made from zinc powder mixed with isopropyl alcohol and Nafion 117 (3 wt %) solution. The Zn slurry was sonicated for 15 minutes before the coating process. The current collector (Cu-Zn mesh) was made from electrodeposition Zn to the Cu mesh.

3.7.2 Ink Preparation

The electrocatalyst metals were dispersed in isopropyl alcohol with Nafion 117 solution as the binder. The desired catalyst loading is 3.0 mg/cm^2. The catalyst slurry was sonicated for 20 minutes before the drop-casting process.

3.7.3 Gas Diffusion Layer preparation

The air electrode was made by drop-casting the catalyst ink on a gas diffusion layer (Freudenberg H26C6, Fuel Cell Store) directly to form a gas diffusion electrode (GDE), followed by drying in the heat plate with the temperature of 60 °C. This process was repeated once to reach a catalyst loading target.

3.7.4 Separator for Zinc Air Battery Cell

For the separator of the zinc air battery, a thin layer of Celgard 5550 was used. The separator was soaked in the electrolyte for 24 hours before assembling the cell.

3.7.5 Fabrication of Zinc Air Battery Cell

In-house zinc-air battery the two-electrode and four-electrode configurations were fabricated by the following procedure. The ZAB cell was made from an acrylic sheet with a thickness of 4 mm. The external cell has a rectangular shape with the size of 4x4 cm^2, as shown in Supplemental material figure 1. This cell has an active area as a circle shape with a diameter of 2 cm. The active area of the cell is 3.14 cm^2. The stainless-steel mesh (40 mesh) was used as a current collector at the air electrode. The electrolyte used was 6 M KOH filled with 0.2 M ZnO to ensure reversible zinc electrochemical reactions at the zinc electrode. The additional reference electrode has been added between the air electrode and separator to present the four-electrode setup. The four-electrode setup has been used to determine the voltage between the air electrode and the reference electrode, which can indicate the electrode degradation when the voltage has been significantly dropped.

3.7.6 Full Cell Testing

The ZAB cell cycle test was carried out on a conventional potentiostat (Gamry 1000). The open circuit potential measurement was used to measure the open-circuit voltage (OCV) of a ZAB cell. The total time of cell voltage measurement is 10 minutes. The OCV of the Zn-Air battery cells in in the rage of 1.35 - 1.60 V. Multistep chronopotentiometry is used to measure the rate of change of potential at an electrode measured at a constant current in which the electrode is charged to a set potential and subsequently discharged. This test was carried out in the range of 5 – 150 mA/cm^2. The current density with the step of 5, 10, 20, 30, 40, 50, 60, 70, 80, 90, 100, 110, 120, 130, 140, and 150 mA/cm^2 were used in this experiment for both discharge and charge. Each current was held at 60 seconds.

Galvanostatic charge/discharge has been used to perform the cell performance test. For the pulse cycling, the cell been tested using air in ambient conditions by the galvanostatic recurrent pulse method with each pulse cycle lasting 10 minutes (5 minutes each for discharge/charge, rest for 1 minute) at a fixed current of 20 mA/cm^2 for 100 cycles. The extended pulse cycling test has been used to study the durability of the cell. The method defined each pulse cycle lasting 6 hours (3 hours each for discharge/charge, rest for 15 minutes) at a fixed current of 20 mA/cm^2.

Chapter 4. Results and Discussion

4.1 Electrical Conductivities of Bifunctional Catalysts

The conductivities of each synthesized catalyst were measured in its powdered form after synthesis. Table 2 provides the conductivities of each sample including industrial benchmark Pt/C Vulcan XC72R. Catalysts with carbon support have the highest electrical conductivity. $NiFe_2O_x$ – unsupported has the smallest electric conductivity. This catalyst is expected to perform the worst in electrocatalytic reactions. Carbon support increased the conductance of catalysts to have similar results to industrial Pt/C Vulcan XC72R. Catalysts without carbon support measured high resistance, confirming transition metal oxides have lower electric conductivity. Catalysts with antimony doped tin oxide supports also measured low conductivity.

Table 2: Conductivities of Catalysts

Sample Number	**Samples**	**Conductance (S/cm)**
#1	$NiCo_5O_x$ - unsupported	4.54×10^2
#2	$NiCo_5O_x$/VulcanXC72R	Highly conductive
#3	$NiCo_5O_x$/VulcanXC72R*	Highly conductive
#4	$NiCo_2O_x$ - unsupported	0.226
#5	$NiFe_2O_x$/VulcanXC72R	Highly conductive
#6	$NiFe_2O_x$ - unsupported	8.96×10^6
#7	$NiFe_2O_x$/VulcanXC72R*	8.348
#8	Pt/C Vulcan XC72R	Highly conductive
#9	Trimetal (Ni, Fe, Co) Oxide with ATO 250CA	0.234
#10	Trimetal (Ni, Fe, Co) Oxide with ATO 251CB	0.160
#11	Trimetal (Ni, Fe, Co) Oxide with ATO 262A	1.590
#12	Trimetal (Ni, Fe, Co) Oxide with ATO 263B	1.120
#13	NiOH and FeO_x with ATO	0.401

4.2 Physical Characterization of Bifunctional Catalysts synthesized by CDTi

Thirteen catalysts were synthesized, and twelve catalysts were analyzed for physical characteristics. X-ray diffraction was used to characterize the elemental composition of the catalysts. The XRD results of all catalysts are shown in Figure 4. Database from the software were able to identify $NiCo_xO_x$ and $NiFe_xO_x$ catalysts in Figure 4A and 4B. Trimetal oxides with antimony tin oxide supports do not show presence of Cobalt. Ratios of #9 - #12 tri-metal oxide are very similar to #8 $NiFeO_x$ on ATO support. Further characterization of tri-metal oxides is performed using SEM and TEM.

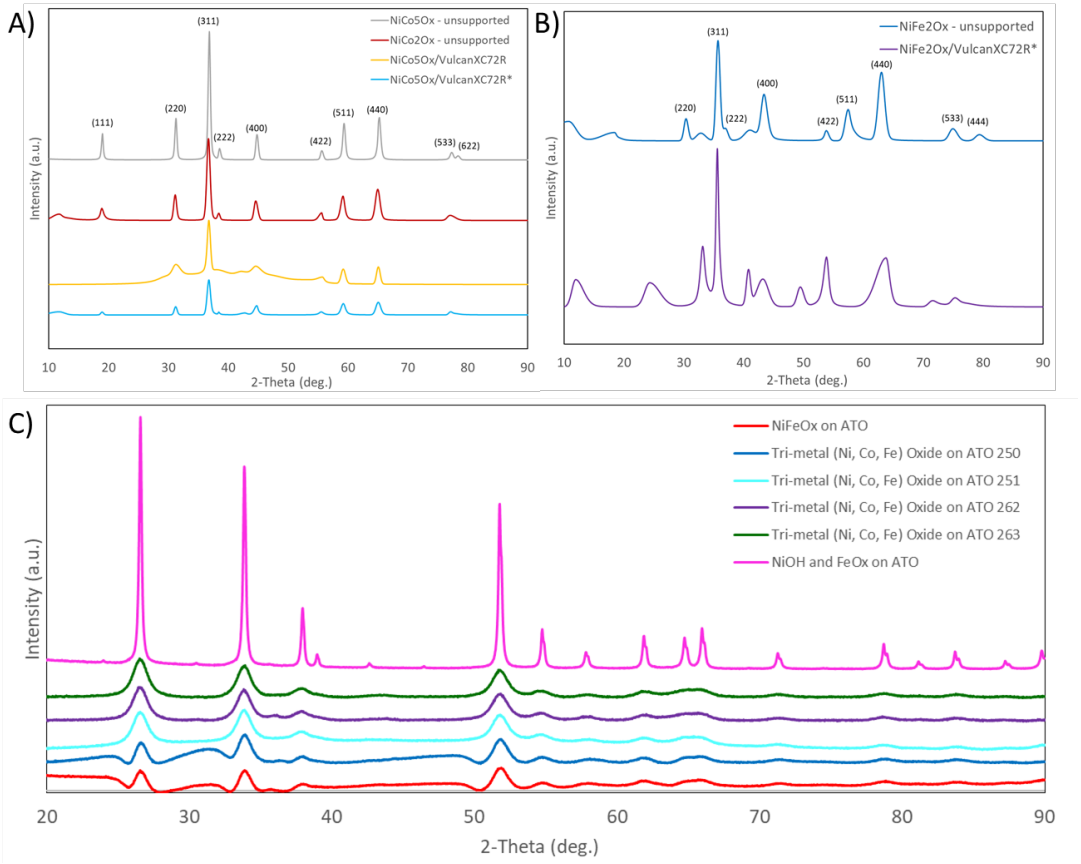

Figure 4. XRD data for A) $NiCo_xO_x$ catalysts, B) $NiFe_xO_x$ catalysts, and C) catalysts with ATO supports.

Morphological properties of the synthesized catalysts were examined by SEM and TEM methods. Fig 5 shows all synthesized catalysts with carbon support and Fig. 6 shows the synthesized catalysts without carbon support. SEM showed catalysts with carbon support have agglomerations of nanostructure particles. Varying particle size distributions and configurations of the catalysts can be examined.

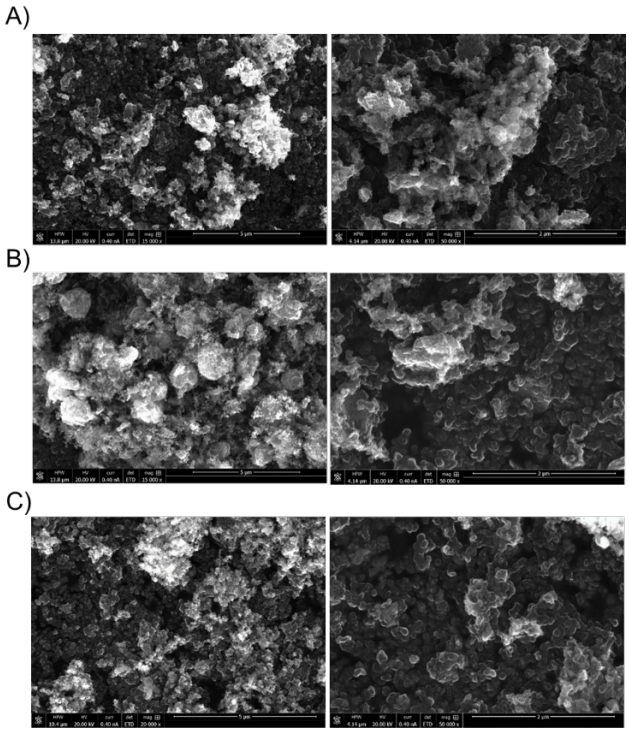

Figure 5. The SEM images of sample A) $NiCo_5O_x$/VulcanXC72R, B) $NiCo_5O_x$ / VulcanXC72R*, and C) $NiFe_2O_x$ / VulcanXC72R.

Spinel structure was achieved with $NiCo_5O_x$ and $NiCo_2O_x$ shown in Fig 6A and 6B. Spinel structure is desired in bifunctional catalysts for electrochemical activity without carbon support. The $NiFe_2O_x$ – unsupported have large particles the size of around 1 micron and are not well-dispersed. This corresponds with Table 2, where $NiFe_2O_x$ – unsupported has the lowest conductivity.

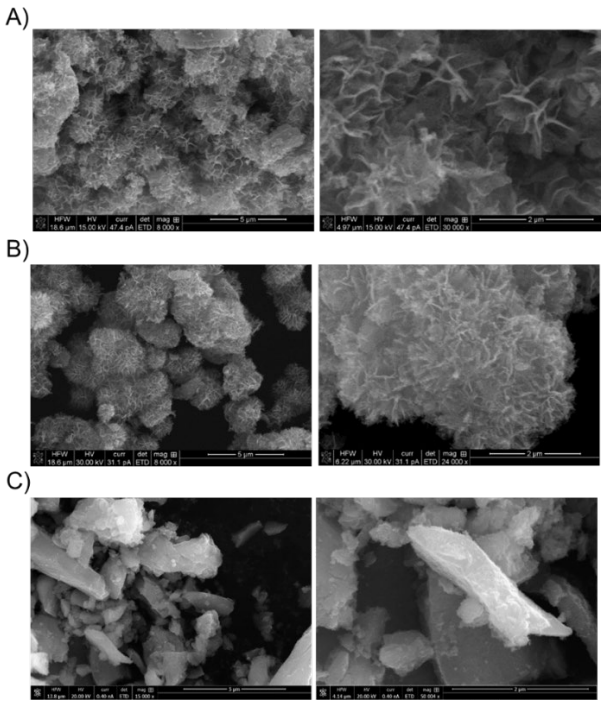

Figure 6. The SEM images of sample A) $NiCo_5O_x$ - unsupported, B) $NiCo_2O_x$ - unsupported, and C) $NiFe_2O_x$ – unsupported.

Figure 7 shows TEM imaging of all the synthesized catalysts with and without carbon support. Amorphous carbon is present and uniform with metal oxides. Particle sizes of catalysts are in good correlation with those observed by SEM. $NiCoO_x$ catalysts consist of particles around 20 nm and $NiFeO_x$ catalysts around 20-25 nm. TEM images show the nickel cobalt oxide and nickel iron oxide samples as agglomerated nanostructures.

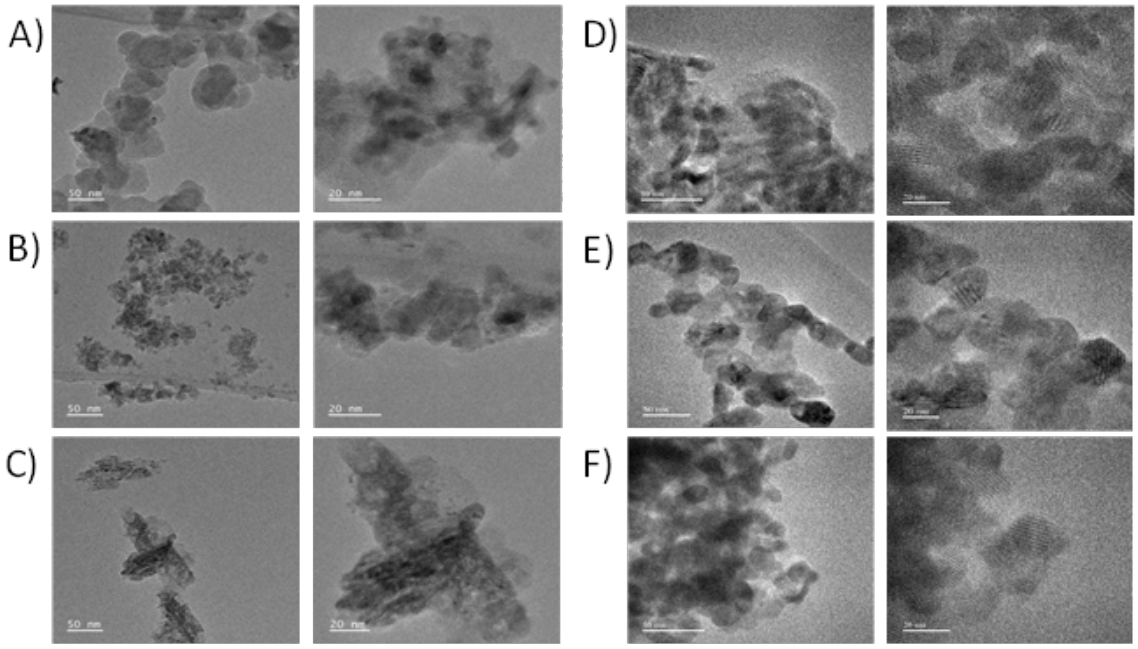

Figure 7. TEM images with 50 nm image scale (left) and 20 nm image scale (right) of A) $NiCo_5O_x$/VulcanXC72R*, B) $NiFe_2O_x$ – unsupported, C) $NiFe_2O_x$/VulcanXC72R, D) $NiCo_5O_x$/VulcanXC72R, E) $NiCo_5O_x$ – unsupported, and F) $NiCo_2O_x$ – unsupported

Among catalysts with ATO supports, #10 Trimetal Oxide with ATO support catalyst was examined for morphological properties due to its best electrocatalytic activity. This is further discussed in section 4.2. Images show various particle sizes of metals. Particles are large similar to $NiFe_2O_x$ – unsupported. Visually, amorphous carbon can be seen in TEM in figure 8B. There is little presence of antimony tin oxide indicating ATO support will not have a strong effect in the metal oxides ORR and OER performance. Spot diffraction analysis was conducted using ImageJ software. The diffraction d-spacing was found to be d = 0.3375 nm.

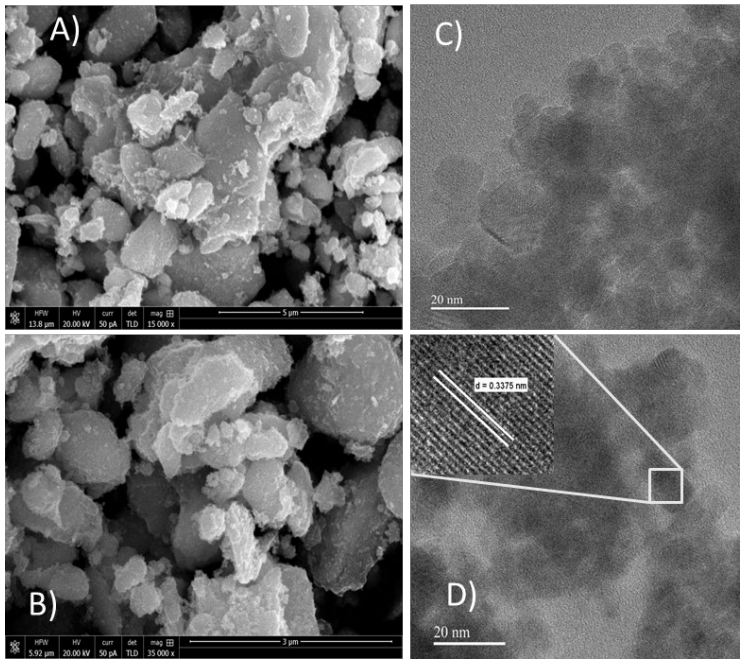

Figure 8. SEM (left column) and TEM (right column) images of #10 Trimetal Oxide on ATO support with A) 5 um image scale, B) 3 um image scale, and C) and D) 20 nm image scale.

4.3 Electrochemical Activity of Catalysts synthesized by CDTi

The electrochemical activity of the library of catalysts is compared. The catalysts were compared to industrial benchmark catalysts Vulcan platinum carbon and iridium oxide for ORR and OER, respectively. The target performance in oxygen reduction reaction is a half-wave potential of 0.93 V displayed by Industrial Pt/C and 1.41 V in oxygen evolution reaction displayed by IrO_x.

The best performers for the cathodic and anodic cycles are the $NiFe_2O_x$ with carbon black support. The poorest performer of this series is $NiFe_2O_x$ – unsupported, as expected from the conductivity and physical characteristics of its morphology and particle size. The ORR and OER LSVs of catalysts without antimony tin oxide supports are shown in Figures 9A and 9B, respectively. In the oxygen reduction reaction activity, $NiCo_5O_x$ supported with Vulcan carbon

performed the best among the novel bifunctional catalysts. $NiCo_5O_x$ displays a half-wave potential of 0.80 V, falling behind Pt/C by 0.1 V. Catalysts with carbon support improved electrochemical activity in ORR. In OER activity, $NiFe_2O_x$ with carbon support performed the best catalytic activity. All catalytic activity performed similarly to industrial level, except for $NiFe_2O_x$ - unsupported. Nickel cobalt catalysts show the addition of carbon support degrades OER performance. However, nickel iron catalysts show an opposite effect where carbon support increases OER activity.

Electrochemical data of catalysts with antimony tin oxide supports is compared with $NiCo_2O_x$ – unsupported as a benchmark for OER activity. The LSVs of catalysts with ATO supports are shown in Figures 9C and 9D. Tri-metal Oxide 251 (cyan) performed the best. Additional LSV trials were conducted and averaged to confirm Tri-metal Oxide 251's high catalytic OER activity (dark red). However, ATO supports did not assist with ORR activity. All catalysts with ATO supports performed less by around 0.2 V in comparison with $NiCo_2O_x$ – unsupported and 0.4 V with Pt/C. To achieve optimal bifunctionality using affordable, obtainable materials unlike platinum, a catalyst must contain Trimetal Oxide with ATO 251 for OER activity and carbon support for best performing ORR.

Although $NiFe_2O_x$ and $NiCo_5O_x$ with carbon supports performed best, carbon corrosion is considered into the integration of battery systems. The electrochemical oxidation of carbon on the electrodes can cause undesirable loss of active species. Thus, the Zn-air battery was tested with pure-metal oxide catalysts: #1 $NiCo_5O_x$ and #6 $NiFe_2O_x$.

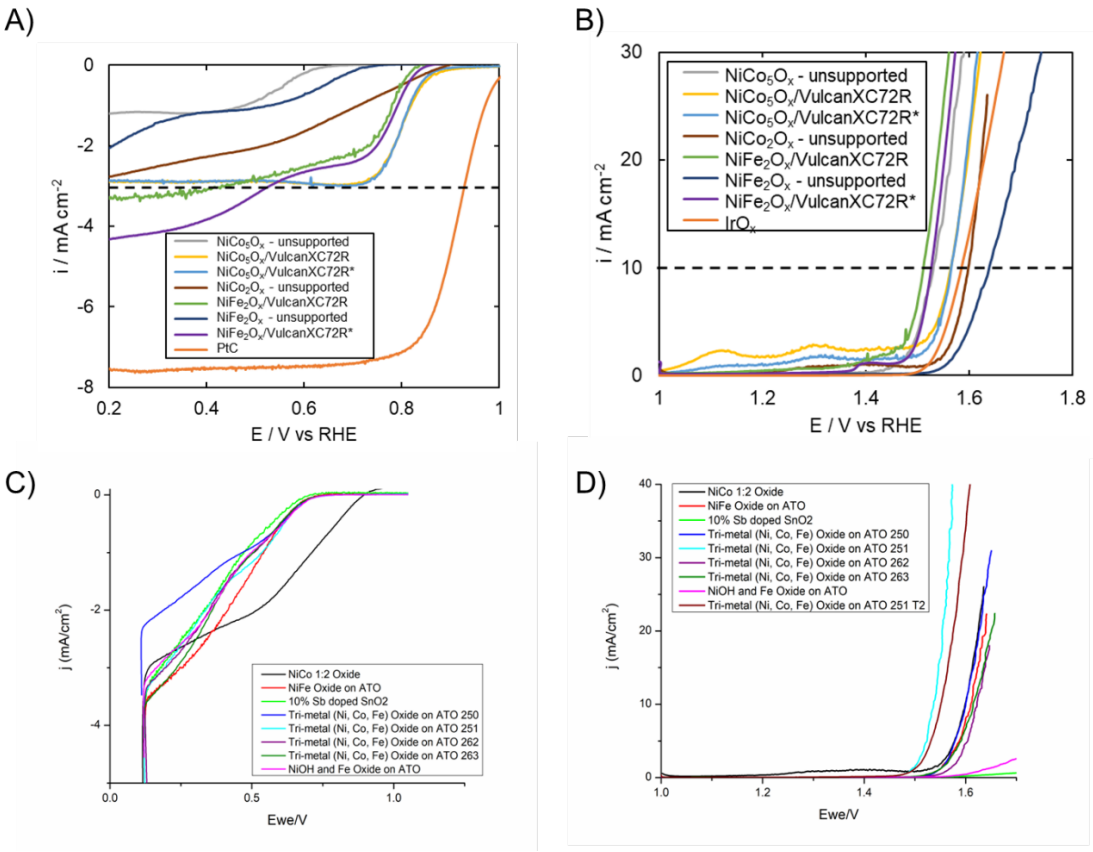

Figure 9. Electrochemical data of PGM free catalysts for ORR and OER in oxygen saturated 1 M KOH at a rotation speed of 1600 rpm with a scan rate of 5 mV/s. A) ORR LSV curves for catalysts without ATO support. B) OER LSV curves for catalysts without ATO support. C) ORR LSV curves for catalyst with ATO support.

Accelerated Stress Tests (AST) can be performed to determine the durability of catalysts. Figure 10 shows the OER performance of $NiCo_5O_x$ – unsupported and $NiFe_2O_x$ – unsupported up to 5000 cycles. Tests confirm there is a drop in performance as the catalyst is cycled more than once. $NiFe_2O_x$ – unsupported shows better durability than $NiCo_5O_x$ - unsupported with less degradation in potential.

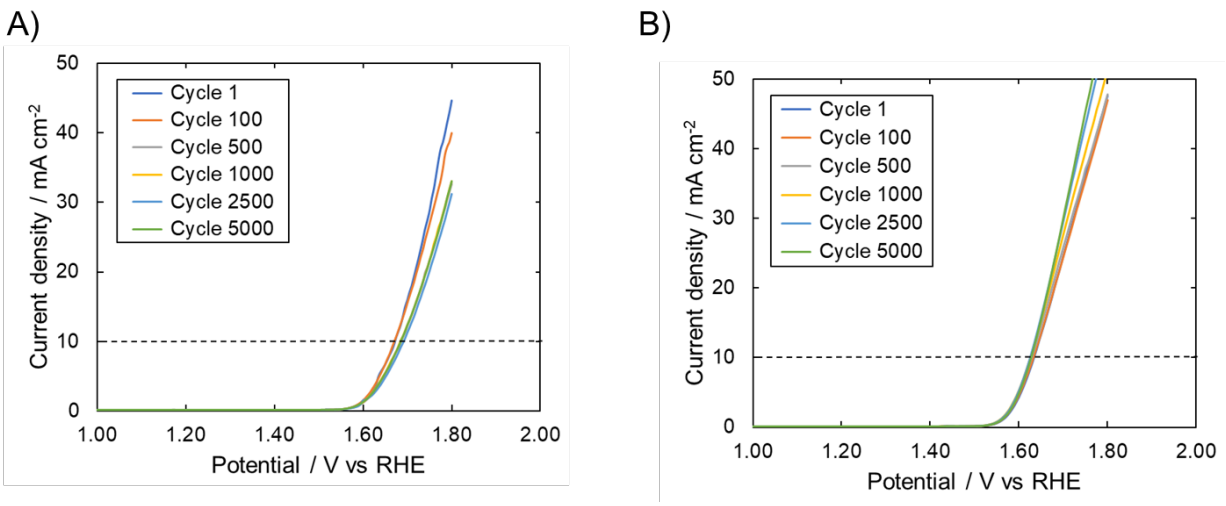

Figure 10. Accelerated stress test (AST) on the RDE in 1 M KOH at a rotation speed of 1600 rpm with the scan rate of 5 mV/s. A) $NiCo_5O_x$ - unsupported B) and $NiFe_2O_x$ – unsupported.

4.4 Rechargeability Testing of Bifunctional Catalysts in ZAB

Figure 11A shows the galvanodynamics discharge and charge polarization curves of ZAB with $NiCo_5O_x$ – unsupported and $NiFe_2O_x$ – unsupported as the OER and ORR bifunctional catalyst comparison to benchmark Pt/C. There is a slightly discharge voltage gap observed for ZAB with both bifunctional catalysts when compared with Pt/C. In comparison with ZAB Pt/C air electrode in a charge polarization profile, both bifunctional catalysts show the lower voltage gap than Pt/C, indicating a better rechargeability. The cycling charge/discharge was performed at the constant current density of 20 mA/cm^2 for these catalysts. Pt/C catalyst ZAB air electrode produced an initial discharge potential of 1.12 V and charge potential of 2.5 V. The ZAB with Pt/C show a slight drop in performance after 20 cycles, indicating low rechargeability and low capacity. The ZAB cell loses all capacity after 60 cycles. This Pt/C air electrode suffered from carbon corrosion, agglomeration of Pt nano particles, and detachment of Pt from the carbon support. These problems indicate performance decay of Pt/C in the air electrode of ZAB. Under the same test

condition, $NiCo_5O_x$ bifunctional catalyst show constant charge/discharge voltage with the initial discharge potential of 1.08 V and charge potential of 2.07 V. This performs higher rechargeability and discharge-ability than Pt/C. $NiFe_2O_x$ shows stable charge/discharge profiles for about the first 10 cycles, then there is a slight voltage drop during discharge indicating lower discharge performance. This cell has an initial discharge/charge potential of 1.03 V and 2.02 V, respectively. However, the ZAB cell has stable charge profile allowing the cell capacity to recharge as the discharge voltage gets higher after several cycles. This bifunctional catalyst has no carbon support, therefore, the ZAB using both bifunctional catalysts air electrode shows a much better cycling durability than that of its counterpart Pt/C catalyst.

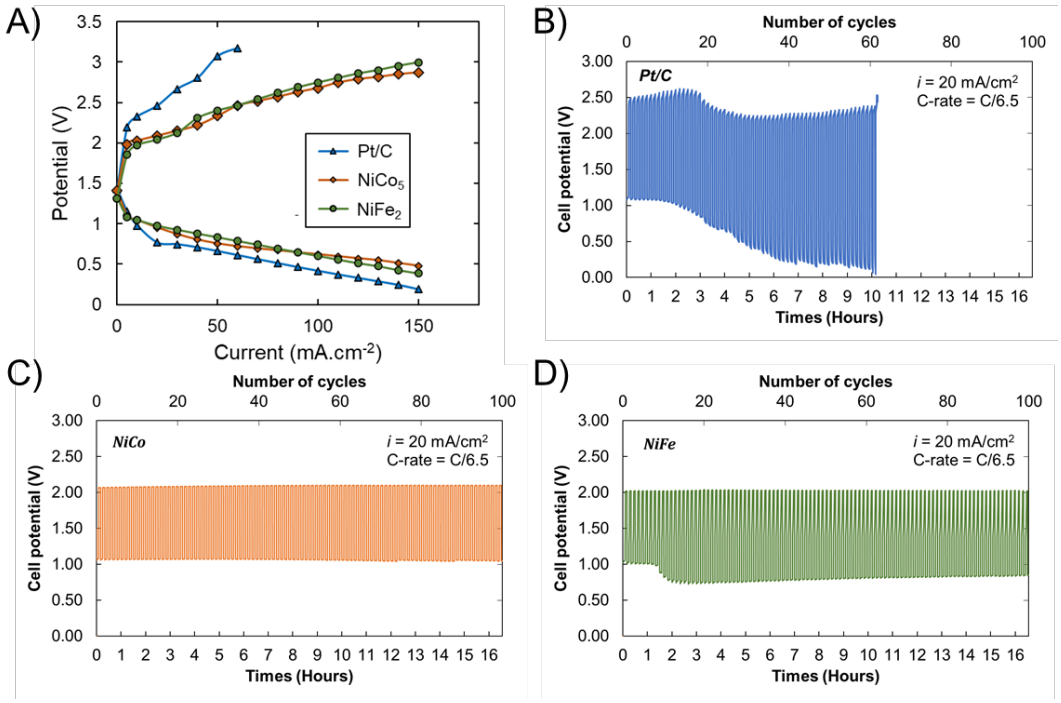

Figure 11. A) Galvanodynamic discharge/charge profiles of zinc air batteries comparison with the catalysts of Pt/C, #1 $NiCo_5O_x$ - unsupported and #6 $NiFe_2O_x$ – unsupported. B) Pulse charging/discharging cycling of PtC catalyst at the current density of 20 mA/cm^2. C) Pulse charging/discharging cycling of #1 $NiCo_5O_x$ - unsupported catalyst at the current density of 20 mA/cm^2. D) Pulse charging/discharging cycling of #6 $NiFe_2O_x$ – unsupported catalyst at the current density of 20 mA/cm^2. Zn foil has been used as a zinc electrode for these tests.

4.5 Physical and Electrochemical Characteristics of $NiCo_5O_x$ – NaOH Method

After completion of physical and electrochemical characterizations of CDTi's catalysts, synthesis of $NiCo_5O_x$ using coprecipitation of NaOH was performed for comparison of different syntheses. The synthesized catalyst was characterized physically using XRD and SEM and electrochemically using RDE.

XRD results are shown in Figure 12. The metal oxide matches $NiCo_2O_4$, but with preferential crystallite orientation indicating a stoichiometric ratio 1:5 nickel to cobalt. Results also correlate to CDTi's synthesized catalyst having the same miller indices.

From SEM analysis, the morphological properties differ. The catalyst structure is more of a mixed metal oxide type than a spinel type. Particle size is much smaller approximately around 0.1 microns. Particles have a wide range of distribution and is evenly dispersed.

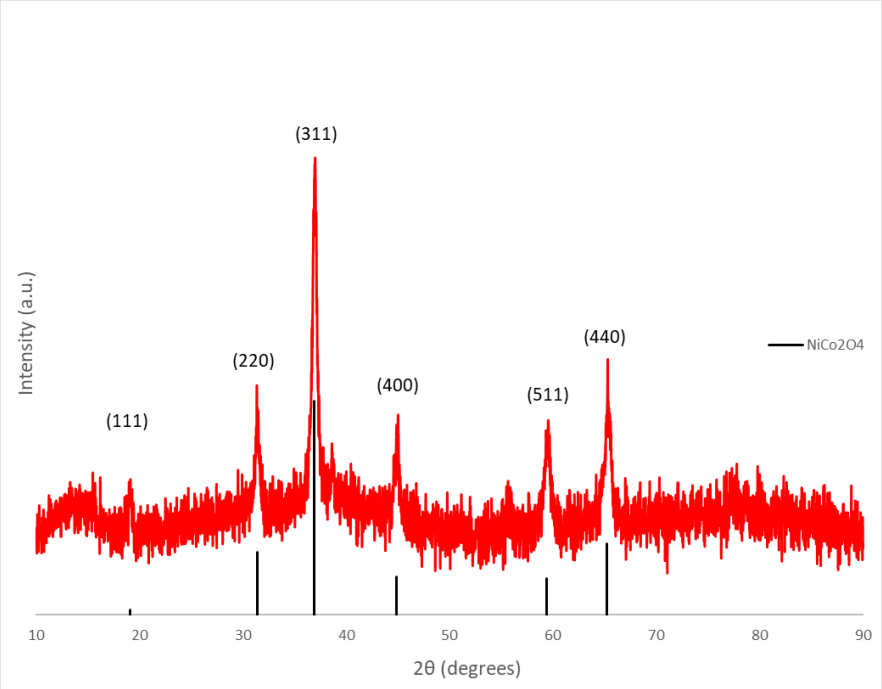

Figure 12. XRD data for $NiCo_5O_x$ – NaOH method

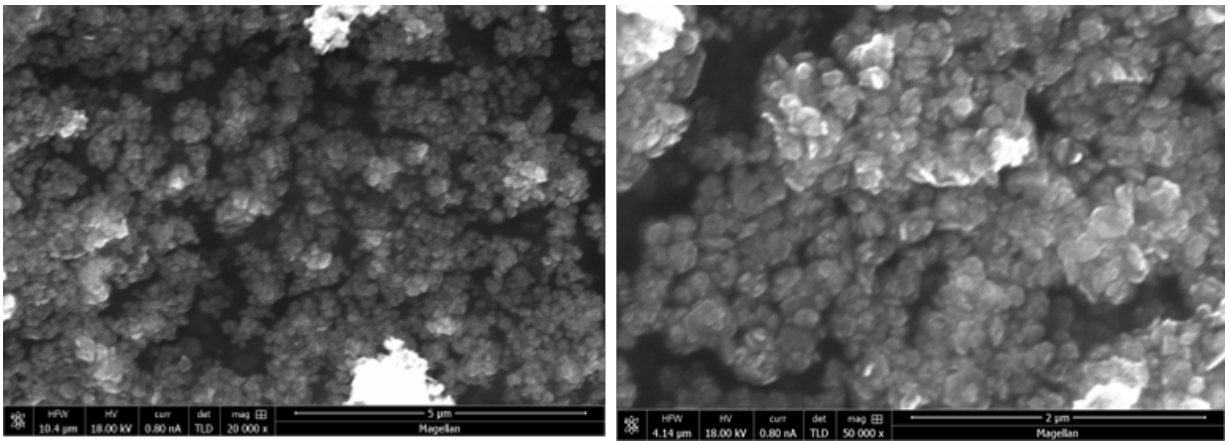

Figure 13. SEM images of $NiCo_5O_x$ – NaOH method with A) 5 um image bar and B) 2 um image bar.

RDE tests were performed in NaCl for analysis in aluminum-air battery. In comparison with 1 KOH $NiCo_5O_x$ – unsupported, the catalyst synthesized using NaOH performs better OER activity in neutral electrolyte. In ORR, the synthesized catalyst using coprecipitation of NaOH has a half potential of 0.25 V, which is 0.3 V less than CDTi's $NiCo_5O_x$ half potential. This is an expected trend where ORR potential is less in neutral electrolyte. Further testing is required before concluding if coprecipitation with NaOH synthesis performs better than CDTi's catalyst.

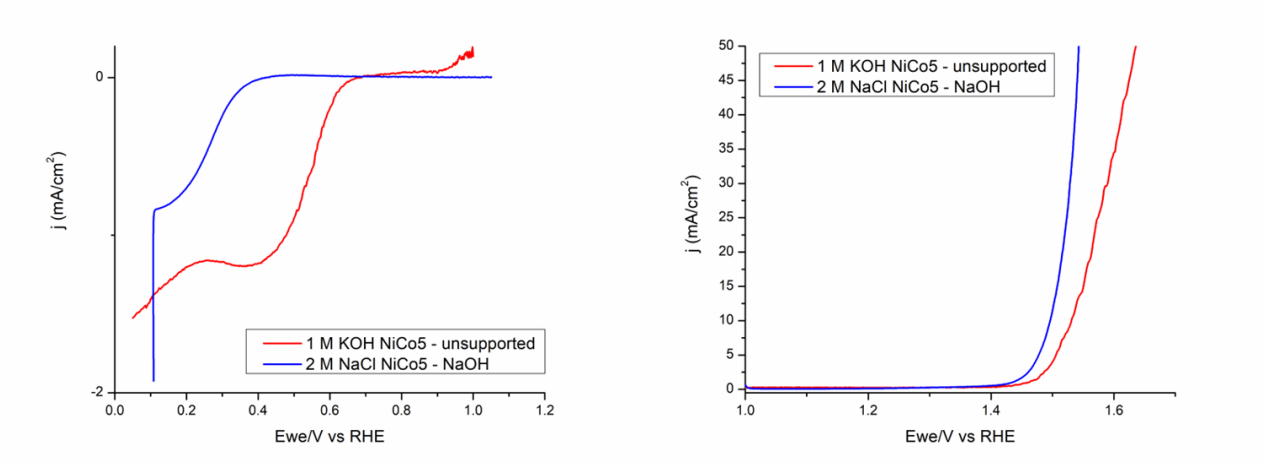

Figure 14. Electrochemical data for $NiCo_5O_x$: A) ORR B) OER

4.6 Electrochemical Testing of $NiCo_5O_x$ with Carbon Support in NaCl Electrolyte

Best performing ORR catalyst $NiCo_5O_x$ with carbon support was selected for further study in the application of bifunctional catalysts in different metal-air batteries.

Electrochemical characterization was conducted using RDE to observe the ORR/OER activity in neutral electrolyte 0.5 M and 2 M NaCl. Electrochemical data is presented in Figure 15. The catalyst performs electrochemically in 0.5 M NaCl. In comparison with basic electrolyte, the ORR performance is very poor, about 0.5 V worse. However, neutral electrolyte is favorable with low CO_2 uptake which allows carbon support catalysts without carbonate effects. Neutral electrolyte is also found to suppress dendrite growth, a common occurrence with carbon corrosion as observed in the ZAB previously mentioned.

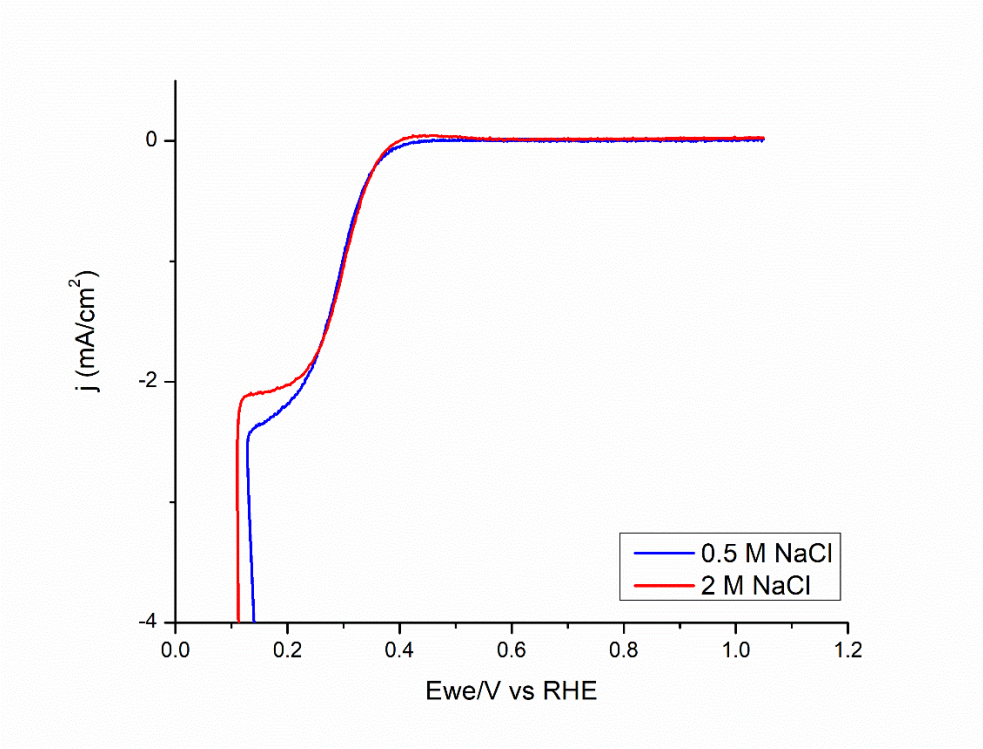

Figure 15. Electrochemical Data for $NiCo_5O_x$ – Carbon Support in electrolyte 0.5 M and 2.0 M NaCl

Chapter 5. Conclusions and Outlook

Bifunctional catalysts provided by CDTi Advanced Materials, Inc. were fully investigated and analyzed physically and electrochemically. Trimetal Oxide with ATO 251 performed the best OER activity. Both $NiCo_5O_x$ with carbon support catalysts have the best ORR activity. The poorest performer of this series in both ORR/OER is $NiFe_2O_x$ – unsupported

In comparison with industrial Pt/C and IrOx catalysts, bifunctional catalyst $NiFe_2O_x$ with carbon support was able to match OER activity of IrOx, with an onset potential of 1.48 V. Trimetal Oxide 251 with ATO support surpassed IrOx OER activity with an onset potential of 1.46 V. The half-wave potential of $NiCo_5O_x$ with carbon support catalyst was found to be 0.8 V, slightly less than Pt/C. The results of all catalysts are tabulated below. All catalysts were tested in 1.0 M KOH.

Table 3. Total Catalyst ORR/OER Data

Sample Number	Catalyst	ORR Half-wave Potential (V)	OER Onset potential vs RHE (V)
#1	$NiCo_5O_x$ - unsupported	0.55	1.42
#2	$NiCo_5O_x$/VulcanXC72R	0.80	1.51
#3	$NiCo_5O_x$/VulcanXC72R*	0.80	1.51
#4	$NiCo_2O_x$ - unsupported	0.30	1.55
#5	$NiFe_2O_x$/VulcanXC72R	0.76	1.48
#6	$NiFe_2O_x$ - unsupported	0.55	1.57
#7	$NiFe_2O_x$/VulcanXC72R*	0.66	1.50
#8	$NiFeO_x$ with ATO	0.41	1.52
#9	Trimetal (Ni, Fe, Co) Oxide with ATO 250	0.28	1.52
#10	Trimetal (Ni, Fe, Co) Oxide with ATO 251	0.33	1.46
#11	Trimetal (Ni, Fe, Co) Oxide with ATO 262	0.32	1.54
#12	Trimetal (Ni, Fe, Co) Oxide with ATO 263	0.33	1.52
#13	NiOH and FeO_x with ATO	0.31	1.60

Catalysts were successfully tested and analyzed in a ZAB. The ZAB tested with Pt/C showed low rechargeability and low capacity. The air electrode also suffered from carbon corrosion and detachment of Pt from carbon support. In comparison to Pt/C, both catalysts performed better rechargeability under the same test conditions. $NiCo_5O_x$ bifunctional catalyst showed constant discharge/charge voltage of 1.08 V and 2.07 V, respectively. $NiFe_2O_x$ bifunctional catalyst has initial discharge/charge voltage of 1.0 3 V and 2.02 V, respectively.

$NiCo_5O_x$ was successfully synthesized using coprecipitation of metal nitrates with NaOH to create a mixed metal oxide bifunctional catalyst.

As an outlook for this research work, with further development and improvement in the oxygen reduction reaction activity, these conductive metal oxides can be used for heavy-duty applications. Antimony tin oxide supports showed to have much better OER performance, but morphology showed the supports were not fully coating the metals. Further development into the synthesis of antimony tin oxide supports needs to be further investigated to confirm the effects of the supports electrochemically. These catalysts can also be tested in aluminum-air battery. Observation of how these catalysts perform in neutral electrolyte can provide further understanding of the catalytic activity in transition metal oxides. Carbon support metal oxides are viable in aluminum-air batteries. Catalyst $NiCo_5O_x$ synthesized by coprecipitation with NaOH can also be further analyzed testing electrochemical activity in basic electrolyte 0.1 M and 1 M KOH for comparison with catalysts with the same structure but synthesized differently. Physical characteristics can also be observed to further understand morphological properties.

References

[1] "May 2022 Monthly Energy Review," U.S. Energy Information Administration. p. 39. 2022.

[2] BP Statistical Review of World Energy & Ember Global Electricity Review (2022)

[3] Maiche, L. French Patent 127,069 1878.

[4] George, W. H. U.S. Patent 1899615 1933

[5] Y. Li, M. Gong, Y. Liang, J. Feng, J.E. Kim, H. Wang, G. Hong, B. Zhang, and H. Dai, Nat Commun, 4, 1805 (2013).

[6] P. Gu, M. Zheng, Q. Zhao, X. Xiao, H. Xue, and H. Pang, J. Mater. Chem. A, 5, 7651-7666 (2017).

[7] F.L Meng, K.H. Liu, Y. Zhang, M.M. Shi, X.B. Zhang, J.M. Yan, and Q. Jiang, Small, 14, 1703843 (2018).

[8] Alexey Serov et al 2015 J. Electrochem. Soc. 162 F449

[9] G. Chai, K. Qiu, M. Qiao, M. Titirci, C. Shang, and Z. Guo, Energy Environ. Sci., 2017, 10, 1186

[10] L. Jorissen. ¨ J. Power Sources. 155, 23 (2006).

[11] Y. Gorlin and T. F. Jaramillo, J. Am. Chem. Soc., 132, 13612 (2010).

[12] G. N. Pirogova, N. M. Panich, R. I. Korosteleva, Y. V. Voronin, and N. N. Popova, Russ. Chem. Bull. Int. Ed., 49, 1536 (2000).

[13] M. Hamdani, R. N. Singh, and P. Chartier, Int. J. Electrochem. Sci., 5, 556 (2010).

[14] C. Jin, F. Lu, X. Cao, Z. Yang, and R. Yang, J. Mater. Chem. A., 1, 12170 (2013).

[15] S. Muller, K. Striebel, and O. Haas, ¨ Electrochim. Acta., 39, 1661 (1994).

[16] O. Haas, F. Holzer, S. Muller, J. M. McBreen, X. Q. Yang, X. Sun, and ¨ M. Balasubramanian, Electrochim. Acta., 47, 3211 (2002).

[17] X. Wu and K. Scott, J. Power Sources., 206, 14 (2012).

[18] M. Bursell, M. Pirjamali, and Y. Kiros, Electrochim. Acta., 47, 1651 (2002).

[19] C. Jin, X. Cao, L. Zhang, C. Zhang, and R. Yang, J. Power Sources., 241, 225 (2013).

[20] Y. Shimizu, K. Uemura, H. Matsuda, N. Miura, and N. Yamazoe, J. Electrochem. Soc., 137, 3430 (1990).

[21] C. Yang and Z. Liu, "Bifunctional OER-ORR electrodes for metal-air batteries," School of Materials, Sun Yat-Sen University (2021)

[22] X. Han, Y. Hu, J. Yang, F. Cheng, J. Chen, Porous perovskite CaMnO3 as an electrocatalyst for rechargeable Li–O2 batteries, Chem. Commun. 50 (12) (2014) 1497–1499.

[23] J.-J. Xu, Z.-L. Wang, D. Xu, F.-Z. Meng, X.-B. Zhang, 3D ordered macroporous LaFeO3 as efficient electrocatalyst for Li–O2 batteries with enhanced rate capability and cyclic performance, Energy Environ. Sci. 7 (7) (2014) 2213–2219.

[24]] F. Cheng, J. Shen, B. Peng, Y. Pan, Z. Tao, J. Chen, Rapid room-temperature synthesis of nanocrystalline spinels as oxygen reduction and evolution electrocatalysts, Nat. Chem. 3 (1) (2010) 79–84.

[25] V. Rai, K.P. Lee, D. Safanama, S. Adams, and D.J. Blackwood, "ORR and OER Bifunctional Electrocatalyst Operating in a Wide pH Range for Cathodic Application in Li-Air Batteries," ACS Appl. Energy Mater. 2020, 3, 9417−9427.

[26] D. Chanda et al., Journal of Power Sources 347 (2017) 247-258.

[27] R. Buckingham et al,. Journal of Power Sources 498 (2021) 229762.